

Enhanced non-macrorealism: Extreme violations of Leggett-Garg inequalities for a system evolving under superposition of unitaries

Arijit Chatterjee[‡],^{1,*} H. S. Karthik[‡],^{2,†} T. S. Mahesh,^{1,‡} and A. R. Usha Devi^{3,§}

¹*Department of Physics and NMR Research Center,*

Indian Institute of Science Education and Research, Pune 411008, India

²*International Centre for Theory of Quantum Technologies, University of Gdansk, 80-308 Gdansk, Poland*

³*Department of Physics, Bangalore University, Bengaluru-560 056, India*

Quantum theory contravenes classical macrorealism by allowing a system to be in a superposition of two or more physically distinct states, producing physical consequences radically different from that of classical physics. We show that a system, upon subjecting to transform under superposition of unitary operators, exhibits enhanced non-macrorealistic feature - as quantified by violation of the Leggett-Garg inequality (LGI) beyond the temporal Tsirelson bound. Moreover, this superposition of unitaries also provides robustness against decoherence by allowing the system to violate LGI and thereby retain its non-macrorealistic behavior for a strikingly longer duration. Using an NMR register, we experimentally demonstrate the superposition of unitaries with the help of an ancillary qubit and verify these theoretical predictions.

Keywords: Leggett-Garg Inequality, Lüder's Bound, Superposition of Unitary, NMR, Decoherence

Introduction—The twilight zone between classical and quantum worlds [1–3] has been under perpetual investigation since the dawn of quantum mechanics [4–6]. The primary foundational difference comes from quantum theory's radical take on 'macrorealism' and 'locality'—two of the most cherished notions of classical physics [4, 5, 7]. The word 'macrorealism' means that a system, capable of being in two or more physically distinct states, will always be in any one of them. This stands in a strong contradiction with quantum theory, which allows the system to be in a superposition of physically distinct states. Superposition of quantum states also permits multiple systems to be in an entangled state [4, 8] where the instantaneous behavior of any one system depends on the other systems even though large distances separate them. This leads to serious debates about the notion of 'locality' [7, 9].

The quantum behaviour of a system is, therefore, primarily accredited to its capability of being in superposition of physically distinct states. Classicality emerges when the system loses the superpositions and turns into an incoherent mixture through decoherence [1, 2, 10, 11]. This can be directly seen through the three-time Leggett-Garg inequality (LGI) [12–14], where the authors considered measuring a dichotomous (± 1 valued) observable \hat{Q} at three different instances t_1, t_2 and t_3 , as the system evolves in time. The quantity of interest here is a linear combination $K_3 := C_{12} + C_{23} - C_{13}$ of two-time correlators $C_{ij} = \langle q(t_i)q(t_j) \rangle$, where $q(t_k) = \pm 1$ is the dichotomic outcome of \hat{Q} at time t_k and $\langle \cdot \rangle$ means

an average over many runs of the experiment. In a classical macrorealistic system, K_3 remains bounded as $-3 \leq K_3 \leq 1$, which is known as 3-term LGI. Quantum systems do not obey classical macrorealism and hence they surpass the upper bound of LGI. Thus the violation of LGI acts as a benchmark of non-classical behavior in terms of non-macrorealism and it is observed experimentally in a variety quantum systems [15–18]. It is also observed [16, 18] that the violation of LGI dies out with time due to decoherence which indicates the emergence of classicality.

These early experiments [15, 16] and theoretical studies [19, 20] suggest that for a two-level quantum system (TLS), evolving under unitary dynamics, the maximum violation of K_3 is constrained by the Temporal Tsirelson bound (TTB), also known as Lüder's Bound, which reads $(K_3)_{\max} \leq 1.5$. This shows that even quantum theory restricts $(K_3)_{\max}$ way below its algebraic maximum value 3. Incidentally, violation of TTB is reported either by replacing the TLS with a multi-level system [21–23] or by replacing unitary evolution with a non-Hermitian \mathcal{PT} symmetric evolution [24–27].

Since the superposition of states allows a system to exhibit non-macrorealistic behavior by violating LGI upto TTB, we ask whether it is possible to get enhanced non-macrorealism that transcends TTB by having superposition not only in the description of state, but also in time evolution unitary! In this work, we investigate time translation of a TLS by subjecting it to an effective unitary transformation achievable via superposition of unitaries and find K_3 violates TTB under such dynamics. In-fact, this enhanced non-macrorealism, as quantified by the violation of LGI beyond TTB, grows with increasing superposition between the unitaries. Furthermore, the unitary superposition provides more robustness to the TLS against decoherence in a noisy environment by allowing it to violate LGI and thereby preserving

[‡] These authors contributed equally to this work

* arijitchattopadhyay01@gmail.com

[†] hsk1729@gmail.com

[‡] tsmahesh@gmail.com

[§] ushadevi@bub.ernet.in

its quantum behavior for a much longer time than usual. We employ Nuclear Magnetic Resonance (NMR) architecture for demonstrating an experimental realization of the superposed unitary operations to verify our theoretical findings. We also provide an intuitive explanation for both the enhanced non-macrorealism and noise robustness in terms of non-linear speed of evolution (SOE) of the TLS arising from the superposition of unitaries.

Superposition of unitaries — In the case of quantum states, the well-known superposition between two physically distinct states, say $|0\rangle$ and $|1\rangle$ ², is formed as $|\psi\rangle = [c_0|0\rangle + c_1|1\rangle]/N$, with $N^2 = \|\tilde{\psi}\|^2$, where $|\tilde{\psi}\rangle := c_0|0\rangle + c_1|1\rangle$ being the unnormalized state. In the same spirit, we propose to form a superposition between two distinct unitary operators $U_0(t_f, t_0) = \exp(-i\hat{\sigma}_n\omega\delta/2)$ and $U_1(t_f, t_0) = \exp(-i\hat{\sigma}_m\omega\delta/2)$, the first one causes a rotation about \hat{n} and the second one about \hat{m} in the Bloch sphere in time $\delta = t_f - t_0$ with frequency ω . Considering $\alpha \in [0, \pi/2]$ as the superposition parameter (SP), the resultant unitary is constructed as

$$\mathcal{U}(t_f, t_0) = \frac{\sin \alpha U_0(t_f, t_0) + \cos \alpha U_1(t_f, t_0)}{\mathcal{N}(t_f, t_0)}, \quad (1)$$

$$\text{with } \mathcal{N}^2(t_f, t_0) = \frac{1}{2} \text{tr} \left[\tilde{\mathcal{U}}(t_f, t_0) \tilde{\mathcal{U}}^\dagger(t_f, t_0) \right], \quad (2)$$

where the unnormalized operator $\tilde{\mathcal{U}}(t_f, t_0)$ is what sits in the numerator of Eq. (1). For the resultant operator $\mathcal{U}(t)$ to be unitary, we need $\tilde{\mathcal{U}}(t_f, t_0)$ to satisfy $\tilde{\mathcal{U}}(t_f, t_0) \tilde{\mathcal{U}}^\dagger(t_f, t_0) \propto \mathbb{1}$, which is true as long as $-1 < \hat{n} \cdot \hat{m} \leq 1$. Note $\mathcal{U}(t_f, t_0) \in SU(2)$ and thus it describes rotation of the Bloch vector in Bloch sphere. Also, $\mathcal{U}(t_f, t_0)$ only depends on $\delta = t_f - t_0$, and not on t_0 .

To construct the general superposed unitary of Eq. (1), consider $\hat{m} = \hat{x}$ and $\hat{n} = \hat{\phi}$, which is a unit vector making an angle $\phi \in [0, \pi)$ with \hat{x} (see Fig. 1 (a)). Taking the initial state of TLS $|\psi\rangle_0 := |0\rangle$, we let it transform under the superposed unitary map as $|\psi\rangle_t = \mathcal{U}(t, 0)|0\rangle = \cos(f(t)/2)|0\rangle - i \sin(f(t)/2) \exp(i\theta)|1\rangle$, where θ depends on α and ϕ . Therefore, if we make t to increase continuously from 0, the map $\mathcal{U}(0, t)$ causes the initial Bloch vector \hat{z} to rotate continuously about an axis $\hat{\theta} = \cos \theta \hat{x} + \sin \theta \hat{y}$. It is crucial to note that this rotation of the Bloch vector happens with a non-linear SOE, which can be defined as $g(t) := \partial_t f(t)$. This $g(t)$ is a non-linear function of t such that the non-linearity increases with increasing SP. Also, the non-linearity in $g(t)$ increases with ϕ , at a given α . Therefore, if we define the superposed unitary of Eq. (1) as a transformation from t_0 to t_f and make t_f to increase continuously, then the action of superposition is two fold : (i) it shifts the

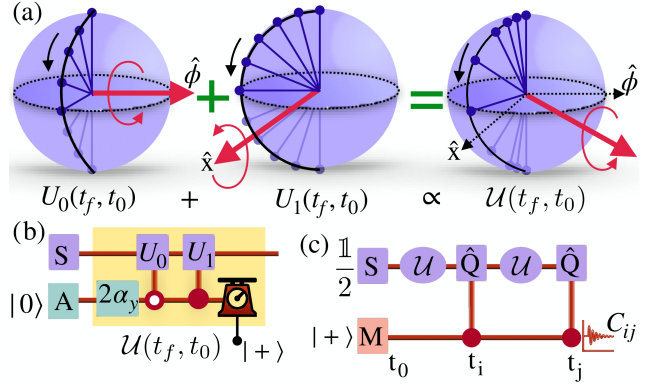


Figure 1. (a) The action of a superposition of two unitaries $U_0 = \exp(-i\hat{\sigma}_\phi\omega\delta/2)$ and $U_1 = \exp(-i\hat{\sigma}_x\omega\delta/2)$ ($\phi = \pi/2$ here) on the Bloch sphere is two fold : Shifting rotation axis (thick arrow) of the effective unitary \mathcal{U} to lie between \hat{x} and $\hat{\phi}$ and making the SOE under it non-linear in time - as the Bloch vector moving slowly near the poles relatively faster near equator. (b) A quantum circuit for realizing the superposed unitary with SP α by using an ancillary qubit (A). Here $2\alpha_y$ describes a rotation of the Bloch vector by angle 2α about \hat{y} . (c) The interferometric circuit to determine the two-time correlator C_{ij} corresponding to observable \hat{Q} using an additional qubit M.

axis of rotation ($\hat{\theta}$) of the Bloch vector to lie in between, and in the same plane of, \hat{n} and \hat{m} , and (ii) it makes the SOE of the Bloch vector to be non-linear in t_f , such that the non-linearity increases with increasing superposition. For a more formal discussion and mathematical proofs, see Appendix A.

Since the superposed unitaries of Eq. (1) do not satisfy the composition law, i.e $\mathcal{U}(t, 0) \neq \mathcal{U}(t, \tau)\mathcal{U}(\tau, 0)$, given $0 < \tau < t$, they are not solutions of Schrödinger equations. Therefore, to realize them, we use an ancillary qubit (A), initialized in a superposed state $|\alpha_A\rangle = \cos \alpha|0\rangle + \sin \alpha|1\rangle$ (see Fig. 1 (b)). In the circuit, two controlled gates $U_{T0}(t_f, t_0) = [U_0(t_f, t_0)]_S \otimes |0\rangle\langle 0|_A + \mathbb{1}_S \otimes |1\rangle\langle 1|_A$ and $U_{T1}(t_f, t_0) = \mathbb{1}_S \otimes |0\rangle\langle 0|_A + [U_1(t_f, t_0)]_S \otimes |1\rangle\langle 1|_A$ are applied back to back. At the end A is post-selected in state $|+\rangle_A := (|0\rangle + |1\rangle)/\sqrt{2}$, which ensures S to transforms as

$$\begin{aligned} \rho_{t_f} &= \frac{\langle +|_A L(t_f, t_0) \rho_{t_0} \otimes |\alpha_A\rangle \langle \alpha_A| L^\dagger(t_f, t_0) |+\rangle_A}{\text{tr} [|+\rangle \langle +|_A L(t_f, t_0) \rho_{t_0} \otimes |\alpha_A\rangle \langle \alpha_A| L^\dagger(t_f, t_0)]} \\ &= \frac{\tilde{\mathcal{U}}(t_f, t_0) \rho_{t_0} \tilde{\mathcal{U}}^\dagger(t_f, t_0)}{\mathcal{N}(t_f, t_0)} = \mathcal{U}(t_f, t_0) \rho_{t_0} \mathcal{U}^\dagger(t_f, t_0), \quad (3) \end{aligned}$$

where $L(\cdot) = U_{T1}(\cdot) U_{T0}(\cdot)$, and ρ_t describes the state of S at time t . Thus, the circuit shown in Fig. 1 (b) describes a physical realization of the system undergoing superposed unitary transformation in time $\delta = t_f - t_0$.

The three-time LGI on a TLS evolving under superposed unitary \mathcal{U} — Choosing $\rho_{t_0} = \mathbb{1}/2$, the two point correlator C_{ij} for dichotomous observable \hat{Q} can be di-

² Throughout this article, $\hat{\sigma}_k$ represents Pauli operator along \hat{k} direction in the Bloch sphere of a TLS, while $|0\rangle$ and $|1\rangle$ are eigenstates of $\hat{\sigma}_z$ with eigenvalues 1 and -1 , respectively

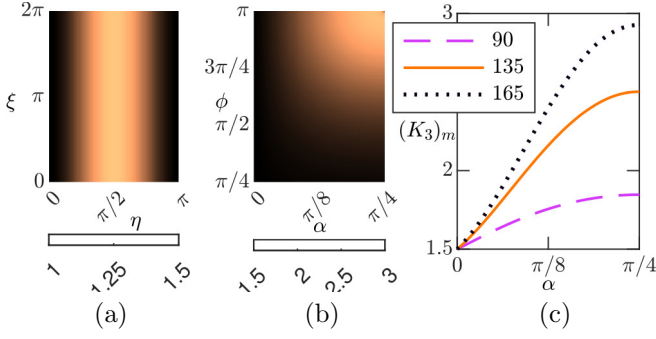


Figure 2. (a) When the system evolves under U_1 , K_3^{\max} is evaluated and color plotted against ξ and η , which are the longitude and co-latitude, respectively, of rotation axis of U_0 on the Bloch sphere. The plot shows K_3 is upper bounded by TTB=1.5. (b) When the system evolves under superposition of unitaries, K_3^{\max} is evaluated and color plotted against α (the amount of superposition) and ϕ (the angle between the rotation axis of the unitaries which are being superposed). For each $\phi \in (0, \pi)$, K_3^{\max} increases with increasing α . (c) The increase of K_3^{\max} with increase in SP α is clearly shown for $\phi = 90^\circ$ (dashed line), $\phi = 135^\circ$ (solid line) and $\phi = 165^\circ$ (dotted line) .

rectly determined using the interferometric circuit [28] shown in Fig. 1 (c). Here the correlation between measurement outcomes of \hat{Q} is stored in the phase of an additional qubit (M), which is initiated in a coherent state $|+\rangle_M$. The measurement outcome of M's coherence $\mathcal{C} := [\langle \hat{\sigma}_x \rangle + i\langle \hat{\sigma}_y \rangle]/2$ directly gives C_{ij} as

$$\text{Re}[\mathcal{C}] = \frac{1}{2} \text{tr} \left[\hat{Q} \mathcal{U}(t_j, t_i) \hat{Q} \mathcal{U}^\dagger(t_j, t_i) \right] = C_{ij}. \quad (4)$$

Note that here the first measurement at time t_i is non-invasive as demanded for an LGI experiment [12–14]. Also, the actual measurement is performed only at the end of the circuit which ensures no post-selection to happen at time t_i .

To evaluate K_3 , we set $\hat{Q} = \hat{\sigma}_z$ and determine the correlators C_{12} , C_{23} and C_{13} for the choice of $t_0 = t_1 = 0$, $t_2 = t$ and $t_3 = 2t$. Since $\mathcal{U}(t_f, t_0)$ of Eq. (1) depends only on $\delta = t_f - t_0$, and not on t_0 , we get $C_{12} = C_{23}$ and $K_3 = 2C_{12} - C_{13}$. First we consider the zero superposition case of $\alpha = 0$. We align the \hat{m} along an arbitrary direction $\hat{m} = \sin \eta \cos \xi \hat{x} + \sin \eta \sin \xi \hat{y} + \cos \eta \hat{z}$ in the Bloch sphere and determine K_3^{\max} over one full cycle $\omega t \in [0, 2\pi]$. We repeat this for each possible $\eta \in [0, \pi]$ and $\xi \in [0, 2\pi]$. The result is shown in Fig. 2 (a) which displays that the K_3^{\max} only depends on η and reaches maximum of $3/2$ when \hat{m} lies in the equator ($\eta = \pi/2$). This confirms the existence of TTB as the upper bound of LGI for any choice of \hat{m} . For non-zero superposition, we consider the general case by aligning \hat{m} and \hat{n} along \hat{x} and $\hat{\phi}$, and compute the maximum K_3^{\max} over one full cycle $\omega t \in [0, 2\pi]$ for full range of parameters $\alpha \in [0, \pi/4]$ and $\phi \in (0, \pi)$. The result is plotted in Fig. 2 (b) which shows increase of K_3^{\max} beyond TTB with increasing α .

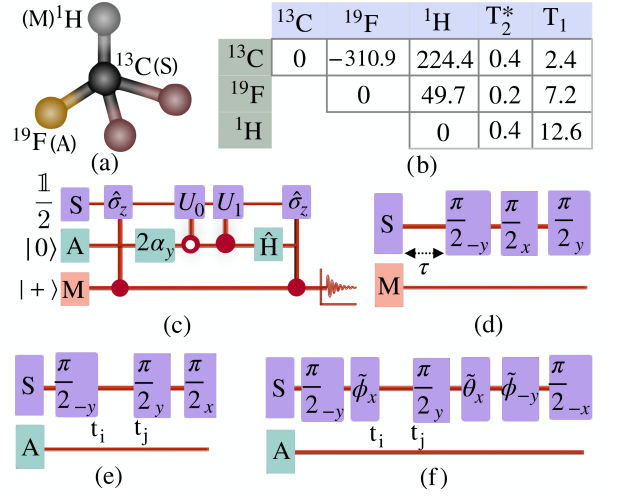


Figure 3. (a) The molecular structure of ^{13}C -DBFM with its qubits labelled. (b) Values of the scalar coupling constants in Hz (J_{ij} in i, j 'th off-diagonal element), resonance offsets (diagonal) along with relaxation time constants (T_1 and T_2^* in s). (c) Quantum circuit for determining C_{ij} of S by measuring the coherence of M in the end. Here \hat{H} signifies a Hadamard gate and $2\alpha_y$ signifies rotation in the Bloch sphere by angle 2α about \hat{y} . (d-f) The quantum circuits used to realize (d) controlled- $\hat{\sigma}_z$ gate (e) U_{T0} and (f) U_{T1} , where $\tilde{\phi} = \phi - \pi$ and $\tilde{\theta} = (\pi - t)/2$. Delays represent evolution under the respective scalar couplings and $\tau = 1/2J_{SM}$. See Appendix B for details.

This growing violation of TTB with rising α is plotted explicitly in Fig. 2 (c) for $\phi = 90^\circ, 135^\circ$ and 165° . These results clearly show that for any given ϕ , the act of superposition in the unitary produces enhanced violation of LGI which increases with increase in the amount of superposition. Moreover, violation of TTB increases with ϕ for a fixed α and K_3 approaches its algebraic maximum $K_3^{\max} = 3$ at $\alpha = \pi/4$ as $\phi \rightarrow \pi$.

Experiments in NMR — Consider the three spin-1/2 nuclei of ^{13}C -dibromofluoromethane (DBFM) molecule as a three qubit quantum register (see Fig. 3 (a)). We identify ^{13}C qubit as our system (S), ^{19}F qubit as A, and ^1H qubit as M. In a strong magnetic field of 11.7 T (along \hat{z}) inside a Bruker 500 MHz NMR spectrometer, the liquid ensemble of ^{13}C -DBFM, dissolved in Acetone- D_6 , rests in thermal equilibrium at an ambient temperature of 300 K. Under high temperature-high field assumption [29], the density matrix of the quantum register reads $\rho_{\text{th}} = \mathbb{1}/8 + \epsilon(\gamma_{\text{C}}I_z^{\text{S}} + \gamma_{\text{F}}I_z^{\text{A}} + \gamma_{\text{H}}I_z^{\text{M}})$, where γ_i is the gyro-magnetic ratio of the i 'th nucleus, $I_z^v := \hat{\sigma}_z^v/2$, and the purity factor $\epsilon \approx 10^{-5}$. Using secular approximation in a triply-rotating frame, rotating at the resonant frequency of each nucleus, the three-qubit quantum register's Hamiltonian can be written as [29, 30] $\mathcal{H}_{\text{NMR}} = 2\pi (J_{\text{SA}}I_z^{\text{S}}I_z^{\text{A}} + J_{\text{SM}}I_z^{\text{S}}I_z^{\text{M}} + J_{\text{AM}}I_z^{\text{A}}I_z^{\text{M}})$, where J 's are the respective scalar coupling constants, values of which along with the relaxation time constants of the quantum register are listed in Fig. 3 (b).

We start the experiment by initializing the quantum

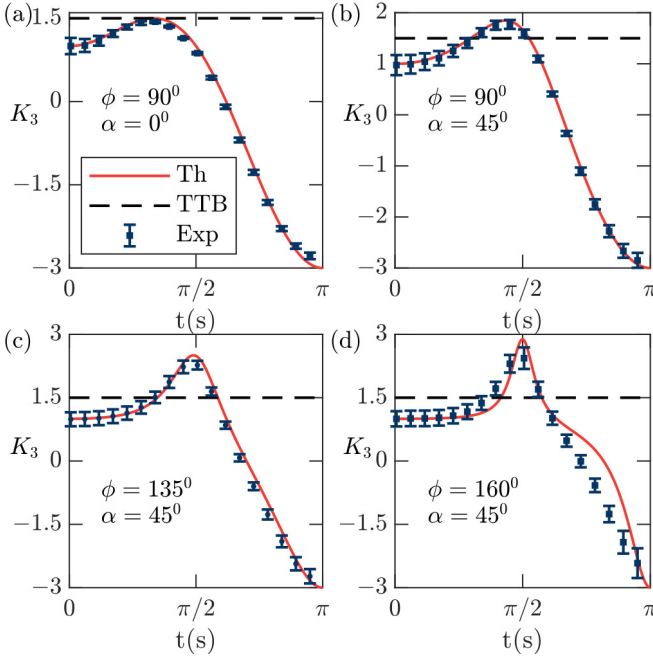


Figure 4. Experimentally measured values of K_3 (dots with vertical error bars) are plotted along with their theoretically predicted curves (solid thin curves) for four different values of α and ϕ . Error bars represent vector sum of systematic (RF in-homogeneity) and random errors (thermal noise).

register in the state $\rho_{in} = (\mathbb{1}/2)_S \otimes |0\rangle\langle 0|_{AM}$ from the thermal state ρ_{th} via preparation of a pseudo-pure state [31, 32] between A and M using spatial averaging with spin selective pulses [33]. After initialization, the quantum circuit of Fig. 3 (c) is used to perform the experiments, where we combine the circuit of Fig. 1 (b) for realizing the superposition of unitaries with the interferometric circuit of Fig. 1 (c) for measuring the correlator C_{ij} . The Hadamard gate \hat{H} on A at the end of the circuit makes post-selecting A in the state $|+\rangle_A$ equivalent to doing the same in state $|0\rangle_A$. A measurement of the real part of the coherence \mathcal{C}_M at the end of the circuit gives

$$\text{Re}[\mathcal{C}_M] = \frac{1}{4}(T_+(t_j, t_i) + T_-(t_j, t_i)) \quad (5)$$

$$\text{where, } T_{\pm}(t_j, t_i) = \text{tr} \left[\hat{\sigma}_z \tilde{U}_{\pm}(t_j, t_i) \hat{\sigma}_z \frac{\mathbb{1}}{2} \tilde{U}_{\pm}^{\dagger}(t_j, t_i) \right],$$

with $\tilde{U}_{\pm} = \cos(\alpha)U_0(t_j, t_i) \pm \sin(\alpha)U_1(t_j, t_i)$. Interestingly, the terms $T_+(t_j, t_i)$ and $T_-(t_j, t_i)$ can be measured separately via distinct spectral lines in NMR, which is equivalent of post selecting A in $\{|0\rangle, |1\rangle\}$ basis. (see Appendix C for details). Just switching off two controlled $\hat{\sigma}_z$ gates, an identical run of the quantum circuit of fig. 3 (c) gives the measurement outcome $\text{Re}[\mathcal{C}_M] = \frac{1}{4}(\mathcal{N}(t_j, t_i) + \tilde{\mathcal{N}}(t_j, t_i))$, with $\mathcal{N}(t_j, t_i)$ as de-

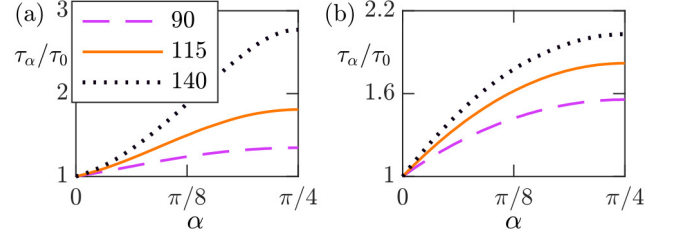


Figure 5. (a) Defining τ_{α} as the time upto which $K_3 \geq 1$, the gain in robustness τ_{α}/τ_0 is computed by solving Eq. (6) and plotted with increasing SP α . The plots are showing increase of τ_{α} with increasing SP for ϕ equals 90° (dashed line), 115° (solid line) and 140° (dotted line), demonstrating the robustness against decoherence due to the superposition of unitaries. (b) The same is plotted, but using a more modest model of Eq. (7), where the additional noise to be encountered in physical realization of the superposition of unitaries are also considered. Results show that the enhanced robustness to persist even in the presence of additional noise. Both computations are done for decay constant $\gamma = 1/(4\pi) \text{ s}^{-1}$.

finied in Eq. (2) and $\tilde{\mathcal{N}}(t_j, t_i) = \sqrt{\text{tr}[\mathcal{U}_-^{\dagger}(t_j, t_i)\mathcal{U}_-(t_j, t_i)]}$. $\mathcal{N}(t_j, t_i)$ and $\tilde{\mathcal{N}}(t_j, t_i)$ can again be measured separately as before. It can be easily seen from Eqs. (1) and (4) that $C_{ij} = T(t_j, t_i)/\mathcal{N}(t_j, t_i)$. This allows direct experimental measurement of C_{ij} by setting appropriate t_i and t_j in the pulse sequence of Fig. 3 (e) and (f). Thus, it works as a general method that effectively realizes the superposed unitary channel $\mathcal{U}(t_j, t_i)$ of Eq. (1). Note that our method allows to choose any value of the SP α and align \hat{n} along any direction by setting appropriate value of α and ϕ in the pulse sequences of Fig. 3 (e) and (f).

We set $t_1 = 0$, $t_2 = t$ and $t_3 = 2t$ as before in our experiments. For no superposition, we set $\alpha = 0$ and measure K_3 while increasing ωt from 0 to π . Results are shown in Fig. 4 (a) confirming the maximum K_3 is exactly the TTB as predicted. Next, we consider the maximum superposition $\alpha = \pi/4$ at $\phi = \pi/2$ and measure K_3 with increasing ωt and observe a clear violation of TTB (see Fig. 4 (b)). We increase ϕ to 135° and 160° at maximum superposition of $\alpha = \pi/4$ and measure K_3 with varying ωt . We observe increasing violation of TTB with increasing ϕ , as predicted theoretically. Experimentally measured value of K_3^{\max} reads 2.27 ± 0.1 for $\phi = 135^\circ$, showing violation of TTB by more than 7 times the experimental uncertainty (Fig. 4 (c)) and 2.43 ± 0.25 for $\phi = 160^\circ$, which violates TTB by more than 3 times the experimental uncertainty (Fig. 4 (d)). These results clearly and convincingly demonstrate the enhanced violation of LGI beyond TTB, due to superposition of unitaries.

We now investigate the effect of markovian dephasing, which is the leading cause of decoherence for most quantum systems, on the dynamics under the superposed unitary. In Eq. (4), the observable $\hat{Q}(0) = \hat{\sigma}_z$ is subjected under $\mathcal{U}(t, 0)$, with choices $\hat{m} = \hat{x}$ and $\hat{n} = \hat{\phi}$, to get transformed to $\hat{Q}(t) = \mathcal{U}(t, 0)\hat{\sigma}_z\mathcal{U}^{\dagger}(t, 0)$. Upon increasing t continuously from 0, this map describes rotation

of the Bloch vector \hat{z} about $\hat{\theta}$ with non-linear SOE $g(t)$. Writing the observable at time t as $\hat{Q}(t) = \vec{S}(t) \cdot \vec{\sigma}$, with Bloch vector $\vec{S}(t) := (S_z(t), S_x(t), S_y(t))$ and Pauli vector $\vec{\sigma} := (\hat{\sigma}_z, \hat{\sigma}_x, \hat{\sigma}_y)$, the rotation is described by the Bloch equation [29, 34], where dephasing can be phenomenologically introduced with decay rate γ as

$$\partial_t \vec{S}(t) = g(t) \hat{\theta} \times \vec{S}(t) - \gamma (\hat{z} \times \vec{S}(t) \times \hat{z}). \quad (6)$$

Eq. (6) is solved with initial condition $\vec{S}(0) = (1, 0, 0)$ to get $\vec{S}(t)$ and $\vec{S}(2t)$, from which we directly compute $K_3(t) = \hat{z} \cdot (2\vec{S}(t) - \vec{S}(2t))$ using Eq. (4). It is expected that decoherence will eventually cause the system to seize to violate LGI and K_3 will fall below the classical bound of 1 as time elapses. The lifetime of the system τ_α is defined as the time up to which K_3 remains above 1 at SP α . We compute the gain in lifetime at SP α as τ_α/τ_0 and plot it with increasing SP for different values of ϕ in Fig. 5 (a). We find the lifetime of the system to enhance significantly with increasing SP, which shows that the act of superposition provides robustness against such dephasing decay and helps the system to retain its quantum behaviour for longer time.

Although the above treatment is mathematically correct, in practice the superposed unitary $\mathcal{U}(t, 0)$ is realized by adding an ancillary system (A) in a coherent state, letting it evolve jointly with S under an interaction Hamiltonian \mathcal{H}_{AS} and finally post-selecting A in $|+\rangle$ state, as shown in Fig. 1 (b). Therefore, in the physical realization of the superposed unitary, S does not evolve directly with a non-linear SOE as described in Eq. (6). It evolves jointly with A until post-selection, and since A is initialized in a coherent state, dephasing will impact A along with S during the course of this joint evolution. To consider that, we subject the joint state ρ_{AS} under a GKSL master equation [35, 36]

$$\partial_t \rho_{AS} = -i[\mathcal{H}_{AS}, \rho_{AS}] + \frac{\gamma}{2} \sum_{j=S,A} (\hat{\sigma}_z^j \rho_{AS} \hat{\sigma}_z^j - \rho_{AS}), \quad (7)$$

where $\hat{\sigma}_z^j$ denotes the action of $\hat{\sigma}_z$ on j and identity on the rest, and the interaction Hamiltonian reads $\mathcal{H}_{AS} := |0\rangle\langle 0| \otimes \omega \hat{\sigma}_n/2 + |1\rangle\langle 1| \otimes \omega \hat{\sigma}_m/2$. In the absence of decoherence ($\gamma = 0$), \mathcal{H}_{AS} generates the joint evolution $\exp(-i\mathcal{H}_T t) = U_{T1}(t, 0) U_{T0}(t, 0)$, which is shown in the circuit of Fig. 1 (b). However, in presence of noise ($\gamma > 0$), and the initial joint state $\rho_{AS}(0) = |\alpha_A\rangle\langle \alpha_A| \otimes \mathbb{1}_S/2$ evolves under Eq. (7) from $t = 0$ to t . After which A is post selected in state $|+\rangle_A$, allowing S to transform under the map $\mathcal{V}(t, 0)$, which describes the effective dynamics under superposed unitary and dephasing. The correlators C_{12} and C_{13} are computed as before with \mathcal{V} replacing \mathcal{U} in Eq. (4). From this we compute $K_3(t)$ to find the gain in lifetime τ_α/τ_0 with increasing SP. Results are plotted for different values of ϕ in Fig. 5 (b), which shows that even the presence of additional noise in A in practical realization protocols does not affect the robust-

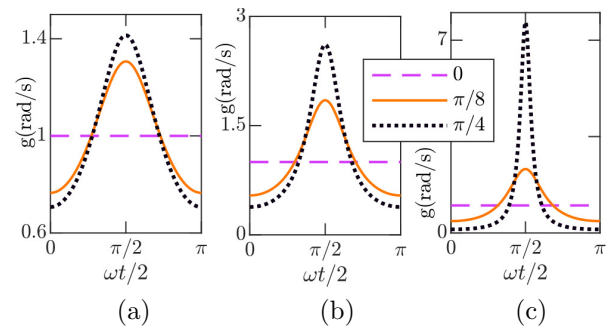


Figure 6. The SOE of a Bloch vector evolving under the superposition of two unitaries for SP $\alpha = 0$ (dashed line), $\pi/8$ (solid line) and $\pi/4$ (dotted line) at (a) $\phi = 90^\circ$, (b) $\phi = 135^\circ$ and (c) $\phi = 165^\circ$. At each ϕ , non-linearity in SOE increases with SP.

ness achieved by the superposition of unitaries against dephasing.

Before concluding, we provide an intuitive way to understand the two main results reported in this article: how the superposition of unitary is causing LGI to go beyond the TTB, and how it is providing the much desired robustness against decoherence. From Eq. (4), it can be directly seen that [20] for $\hat{Q} = \hat{\sigma}_z$, $C_{ij} = \mathcal{U}(t_j, t_i)[\hat{z}] \cdot \hat{z}$, where \hat{z} is the initial Bloch vector at time t_i , representing the observable, which gets rotated to $\mathcal{U}(t_j, t_i)[\hat{z}]$ at time t_j in Heisenberg picture. At zero superposition, $\mathcal{U}(t_j, t_i)$ describes rotation at frequency ω about an arbitrary axis. Therefore, for our choice of $t_0 = t_1 = 0$, $t_2 = t$ and $t_3 = 2t$, if it rotates \hat{z} by an angle $\omega t/2$ in time t , the rotation in time $2t$ will be ωt , resulting $K_3 = 2 \cos(\omega t/2) - \cos(2\omega t)$, which always remains upper bounded by 1.5 for any ωt . This shows that TTB originates from the linearity of rotation of the Bloch vector and necessitates a non-linear SOE for the violation of TTB. As an example, for K_3 to approach its algebraic maximum 3, we need C_{12} and C_{13} to approach 1 and -1 , respectively, at same value of t . This requires \mathcal{U} to rotate the vector \hat{z} almost none in 0 to t but by an angle π from t to $2t$ which can only be performed with extreme non-linear SOE. We plot the SOE of the Bloch vector \hat{z} at different values of the α , for $\phi = 90^\circ$, 135° and 165° in Fig. 6 (a), (b) and (c), respectively. The figure displays the SOE getting increasingly non-linear with increasing SP for each value of ϕ , which correspondingly results enhanced violation of TTB with increasing α . The robustness against dephasing can also be understood with the same argument. The effect of decoherence increases with increasing co-latitude of the Bloch sphere-dephasing has no effect on the poles and does maximum damage on the equator. Due to non-linearity in the SOE, the Bloch vector spends lesser time in the equator and remains longer near the pole, thereby saving itself from decoherence. This explains the increased robustness of the system with increasing superposition between the unitaries as described by Eq. (6). Also, Fig. 6 shows that

at a given α , the non-linearity in SOE increases with increasing ϕ , which explains the increasing violation of TTB in Fig. 4 (c-d) and increasing robustness against dephasing in Fig. 5 (a-b) at maximum superposition, with increasing ϕ .

Conclusions– The drastic contrast between the classical and quantum worlds originates primarily from the ability of quantum systems to be in a superposition of physically distinct states. This breach of ‘macrorealism’ as the source of quantum behavior was quantified with a violation of LGI up-to TTB and has been experimentally confirmed in many quantum systems. The question arises whether we get a quantum behavior showcasing enhanced non-macrorealism if we apply the superposition principle not only in the description of states but also in the time evolutions. By constructing unitary operators that can be written as superpositions of other unitaries and letting a quantum system evolve under it, we observe that the system exhibits enhanced violation of LGI that surpasses TTB. We quantify this experimentally and show that the violation increases with increasing superposition between the unitaries. Moreover, we found that the act of superposition has application in providing robustness against decoherence by substantially extending the system’s lifetime. Both of these enhanced temporal correlations in terms of LGI and robustness against noise can be attributed to the non-linear SOE arising because of the superposition of unitaries. Our work paves the way for research regarding the implications of this new dynamics under the superposed unitaries across different areas of physics.

Acknowledgments.– AC acknowledges Vishal Varma for useful suggestions regarding software setting of the plots. HSK thanks NCN Poland, ChistEra-2023/05/Y/ST2/00005 under the project Modern Device Independent Cryptography (MoDIC). T.S.M. acknowledges funding from DST/ICPS/QuST/2019/Q67 and I-HUB QTF. ARU is

funded by DST/ICPS/QuST/2019/Q107.

Appendix A: Properties of the superposed unitaries and defining the SOE

As mentioned in the main text, we take two arbitrary directions $\hat{n} = n_x\hat{x} + n_y\hat{y} + n_z\hat{z}$ and $\hat{m} = m_x\hat{x} + m_y\hat{y} + m_z\hat{z}$ in the Bloch sphere. We then construct a superposition between $U_0(t_f, t_0) = \exp(-i\hat{\sigma}_n\omega\delta/2)$ and $U_1(t_f, t_0) = \exp(-i\hat{\sigma}_m\omega\delta/2)$ according to Eq. (1) of main text to form $\mathcal{U}(t_f, t_0)$. The unnormalized operator reads

$$\begin{aligned}\tilde{\mathcal{U}}(t_f, t_0) &= \sin(\alpha)U_0(t_f, t_0) + \cos(\alpha)U_1(t_f, t_0) \\ &= (\sin(\alpha) + \cos(\alpha)) \cos \frac{\omega\delta}{2} \mathbb{1} \\ &\quad -i (\sin(\alpha)\hat{\sigma}_n + \cos(\alpha)\hat{\sigma}_m) \sin \frac{\omega\delta}{2}.\end{aligned}\quad (\text{A1})$$

Using this, we find

$$\begin{aligned}\tilde{\mathcal{U}}(t_f, t_0)\tilde{\mathcal{U}}^\dagger(t_f, t_0) &= \\ \underbrace{\left[1 + \sin(2\alpha) \left(\cos^2 \frac{\omega\delta}{2} + \hat{n} \cdot \hat{m} \sin^2 \frac{\omega\delta}{2} \right) \right]}_{\mathcal{N}(t_f, t_0)} \mathbb{1},\end{aligned}\quad (\text{A2})$$

which ensures that the superposed operator $\mathcal{U}(t_f, t_0) = \tilde{\mathcal{U}}(t_f, t_0)/\sqrt{\mathcal{N}(t_f, t_0)}$ is always an unitary operator for arbitrary values of t_f and t_0 and for arbitrary choices of directions \hat{n} , \hat{m} , as long as $-1 < \hat{n} \cdot \hat{m} \leq 1$, which is required to ensure the positivity of $\mathcal{N}(t_f, t_0)$ for all values of t_0 , t_f and $\alpha \in [0, \pi/4]$.

Without loss of generality, we consider $\hat{m} := \hat{x}$ and $\hat{n} := \hat{\phi}$ as in the main text, where $\hat{\phi}$ is a unit vector making an angle $\phi \in [0, \pi)$ with \hat{x} . Taking, $t_0 = 0$ and $t_f = t$, the superposed unitary can be expanded as

$$\begin{aligned}\mathcal{U}(t, 0) &= \frac{\begin{bmatrix} (\cos \alpha + \sin \alpha) \cos \frac{\omega t}{2} & -i (\cos \alpha + e^{-i\phi} \sin \alpha) \sin \frac{\omega t}{2} \\ -i (\cos \alpha + e^{i\phi} \sin \alpha) \sin \frac{\omega t}{2} & (\cos \alpha + \sin \alpha) \cos \frac{\omega t}{2} \end{bmatrix}}{\sqrt{1 + \sin(2\alpha) [\cos^2 \frac{\omega t}{2} + \cos \phi \sin^2 \frac{\omega t}{2}]}} = \frac{(\cos \alpha + \sin \alpha) \cos \frac{\omega t}{2}}{\underbrace{\sqrt{1 + \sin(2\alpha) [\cos^2 \frac{\omega t}{2} + \cos \phi \sin^2 \frac{\omega t}{2}]}_{\cos[f(t)/2}}} \mathbb{1} \\ &\quad -i \underbrace{\frac{\sqrt{1 + \cos \phi \sin(2\alpha)} \sin \frac{\omega t}{2}}{\sqrt{1 + \sin(2\alpha) [\cos^2 \frac{\omega t}{2} + \cos \phi \sin^2 \frac{\omega t}{2}]}}_{\sin[f(t)/2]} \left(\underbrace{\frac{\cos \alpha + \cos \phi \sin \alpha}{\sqrt{1 + \cos \phi \sin(2\alpha)}}}_{\cos \theta} \hat{\sigma}_x + \underbrace{\frac{\sin \alpha \sin \phi}{\sqrt{1 + \cos \phi \sin(2\alpha)}}}_{\sin \theta} \hat{\sigma}_y \right) = \cos \left[\frac{f(t)}{2} \right] \mathbb{1} - i \sin \left[\frac{f(t)}{2} \right] \hat{\sigma}_{\text{SP}},\end{aligned}$$

where $\hat{\sigma}_{\text{SP}} := \cos \theta \hat{\sigma}_x + \sin \theta \hat{\sigma}_y$. To define the speed of evolution (SOE) $g(t)$, we take the initial state $|\psi_0\rangle := |0\rangle$

and let it transform under the superposed unitary as

$$\begin{aligned}|\psi_t\rangle &= \mathcal{U}(t, 0)|0\rangle = \cos \left[\frac{f(t)}{2} \right] |0\rangle - i \sin \left[\frac{f(t)}{2} \right] e^{i\theta} |1\rangle \\ &= \cos \left[\frac{f(t)}{2} \right] |0\rangle + \sin \left[\frac{f(t)}{2} \right] e^{i(\theta - \pi/2)} |1\rangle.\end{aligned}\quad (\text{A3})$$

Therefore, if we increase t continuously from 0, Eq. (A3) describes counter-clockwise rotation of the Bloch vector \hat{z} about axis $\hat{\theta} := \cos\theta\hat{x} + \sin\theta\hat{y}$ in the Bloch Sphere. SOE ($g(t)$) can now be defined as the rate of change of the co-latitude (which is the only degree of freedom that is changing here) of the Bloch vector with t as

$$g(t) = \partial_t f(t) = \frac{-2\partial_t \cos[f(t)/2]}{\sin[f(t)/2]}. \quad (\text{A4})$$

Computing the derivatives, we get

$$\begin{aligned} & \partial_t \cos[f(t)] \\ = & -\frac{\omega(1 + \sin(2\alpha)\cos\phi)(\cos\alpha + \sin\alpha)\sin\frac{\omega t}{2}}{[1 + \sin(2\alpha)(\cos^2\frac{\omega t}{2} + \cos\phi\sin^2\frac{\omega t}{2})]^{3/2}}, \end{aligned} \quad (\text{A5})$$

which directly gives a closed form expression for the SOE. Of course, SOE can be defined more generally by taking a generic initial state as $|0\rangle$ instead of $|0\rangle$. In that case, both the co-latitude and longitude of the Bloch vector will change with t , and therefore $g(t)$ will read as the magnitude of the vector sum of these two rate of changes. However, the special case presented here suffices the requirements of this paper.

Appendix B: Detailed Derivations of the Quantum Circuits Used

Here we derive the pulse sequence for the controlled gates used in the quantum circuit shown in Figure 3 (d-f) in the main text. We denote $|0\rangle\langle 0| := \sigma_0$ and $|1\rangle\langle 1| := \sigma_1$. For the controlled $\hat{\sigma}_z$ gate, note

$$\begin{aligned} U_{cz} &= \mathbb{1}_S \otimes |0\rangle\langle 0|_M + \hat{\sigma}_z^S \otimes |1\rangle\langle 1|_M \\ &= \sigma_0^M + \sigma_z^S \sigma_1^M = e^{i\sigma_z^S \sigma_1^M \pi/2} = e^{i\sigma_z^S \pi/4} e^{-i\sigma_z^S \sigma_z^M \pi/4} \\ &= e^{-i\sigma_y^S \pi/4} e^{-i\sigma_x^S \pi/4} e^{i\sigma_y^S \pi/4} e^{-i\sigma_z^S \sigma_z^M \pi/4}, \end{aligned} \quad (\text{B1})$$

which is the circuit shown in Fig. 3 (d) in the main text.

Now, we note

$$\begin{aligned} U_{T0} &= (e^{-i\sigma_x \omega t/2})_S \otimes |0\rangle\langle 0|_A + \mathbb{1}_S \otimes |1\rangle\langle 1|_A \\ &= \sigma_1^A + \cos(\omega t/2)\sigma_0^A - i\sin(\omega t/2)\sigma_x^S \sigma_0^A \\ &= e^{-i\sigma_0^A \sigma_x^A \omega t/2} = e^{-i\sigma_x^S (1+\sigma_z^A) \omega t/4} \\ &= e^{-i\sigma_x^S \omega t/4} e^{-i\sigma_y^S \pi/4} e^{-i\sigma_z^S \sigma_z^A \omega t/4} e^{i\sigma_y^S \pi/4}, \end{aligned} \quad (\text{B2})$$

which is the pulse sequence shown in Fig 3 (e) in the

main text. By a similar line of reasoning, we find

$$\begin{aligned} U_{T1} &= (e^{-i\sigma_\phi \omega t/2})_S \otimes |1\rangle\langle 1|_A + \mathbb{1}_S \otimes |0\rangle\langle 0|_A \\ &= \sigma_0^A + \cos(\omega t/2)\sigma_1^A - i\sin(\omega t/2)\sigma_\phi^S \sigma_0^A \\ &= e^{-i\sigma_1^A \sigma_\phi^S \omega t/2} = e^{-i\sigma_\phi^S (1-\sigma_z^A) \omega t/4} \\ &= e^{-i\sigma_\phi^S \omega t/4} e^{i\sigma_z^S (\pi-\phi)/2} e^{-i\sigma_x^S \sigma_z^A \omega t/4} e^{-i\sigma_z^S (\pi-\phi)/2} \\ &= e^{i\sigma_z^S (\pi-\phi)/2} e^{i\sigma_x^S \omega t/4} e^{-i\sigma_y^S \pi/4} e^{-i\sigma_z^S \sigma_z^A \omega t/4} e^{i\sigma_y^S \pi/4} e^{-i\sigma_z^S (\pi-\phi)/2} \\ &= e^{i\sigma_x^S \pi/4} e^{-i\sigma_y (\pi-\phi)/2} e^{i\sigma_x^S (\omega t-\pi)/4} e^{-i\sigma_y^S \pi/4} e^{-i\sigma_z^S \sigma_z^A \omega t/4} \\ & \quad e^{i\sigma_x^S (\pi-\phi)/2} e^{i\sigma_y^S \pi/4}, \end{aligned} \quad (\text{B3})$$

which is the pulse sequence shown in Fig 3 (f) in the main text.

Appendix C: Experimental Details

Here we first derive the Eq. (5) of the main text. Evolution of the quantum register under the quantum circuit shown in Fig 3 (c) in the main text reads :

$$\begin{aligned} & \frac{1}{2} (|0\rangle\langle 0| + |1\rangle\langle 1| + |0\rangle\langle 1| + |1\rangle\langle 0|)_M \\ & \otimes (\cos^2(\alpha)|0\rangle\langle 0| + \sin^2(\alpha)|1\rangle\langle 1| + \cos(\alpha)\sin(\alpha)(|0\rangle\langle 1| + \\ & \quad |1\rangle\langle 0|))_A \otimes \frac{\mathbb{1}}{2}_S \\ & \quad \downarrow [U_{T0} U_{T1}]_{AS} \\ & \frac{1}{2} (\dots + |0\rangle\langle 1| + |1\rangle\langle 0|)_M \otimes (\cos^2(\alpha)|0\rangle\langle 0|_A \otimes [U_{T0} \frac{\mathbb{1}}{2} U_{T0}^\dagger]_S \\ & \quad + \sin^2(\alpha)|1\rangle\langle 1|_A \otimes [U_{T1} \frac{\mathbb{1}}{2} U_{T1}^\dagger]_S + \cos(\alpha)\sin(\alpha) \\ & \quad |0\rangle\langle 1|_A \otimes [U_{T0} \frac{\mathbb{1}}{2} U_{T1}^\dagger]_S + |1\rangle\langle 0|_A \otimes [U_{T1} \frac{\mathbb{1}}{2} U_{T0}^\dagger]_S) \\ & \quad \downarrow \hat{H}_A \rightarrow \text{tr}_{AS}[\cdot] \\ & \rho_M = \frac{1}{2} |+\rangle\langle +| (T_+ + T_-), \end{aligned} \quad (\text{C1})$$

which results the (real) NMR signal $S = \text{tr}[\sigma_x \rho_M] = \frac{1}{4}(T_+ + T_-)$ when M is measured. This completes the derivation of Eq. (5) in the main text. Just following these line of steps, the similar results for \mathcal{N} of the main text can also be derived directly.

Finally, note that during NMR signal acquisition, the final three qubit state effectively evolves under \mathcal{H}_{NMR} of the main text. This causes the T_+ and T_- of Eq. (C1) to evolve at different frequencies. Therefore by taking a Fourier transform of the time domain signal we go to the frequency domain where we find T_+ and T_- to be separated. This allows us to post-select the T term.

[1] W. H. Zurek, Decoherence, einselection, and the quantum origins of the classical, *Rev. Mod. Phys.* **75**, 715

(2003).

[2] W. H. Zurek, Preferred states, predictability, classicality

- and the environment-induced decoherence, *Progress of Theoretical Physics* **89**, 281 (1993).
- [3] W. H. Zurek, Quantum darwinism, classical reality, and the randomness of quantum jumps, *Physics today* **67**, 44 (2014).
- [4] A. Einstein, B. Podolsky, and N. Rosen, Can quantum-mechanical description of physical reality be considered complete?, *Phys. Rev.* **47**, 777 (1935).
- [5] J. S. Bell, On the einstein podolsky rosen paradox, *Physics Physique Fizika* **1**, 195 (1964).
- [6] R. P. Feynman and F. L. Vernon Jr, The theory of a general quantum system interacting with a linear dissipative system, *Annals of physics* **281**, 547 (2000).
- [7] A. Aspect, J. Dalibard, and G. Roger, Experimental test of bell's inequalities using time-varying analyzers, *Phys. Rev. Lett.* **49**, 1804 (1982).
- [8] R. Horodecki, P. Horodecki, M. Horodecki, and K. Horodecki, Quantum entanglement, *Rev. Mod. Phys.* **81**, 865 (2009).
- [9] J.-W. Pan, D. Bouwmeester, M. Daniell, H. Weinfurter, and A. Zeilinger, Experimental test of quantum nonlocality in three-photon greenberger–horne–zeilinger entanglement, *Nature* **403**, 515 (2000).
- [10] K. Hornberger, Introduction to decoherence theory, in *Entanglement and Decoherence: Foundations and Modern Trends* (Springer, 2009) pp. 221–276.
- [11] E. Joos, H. D. Zeh, C. Kiefer, D. J. Giulini, J. Kupsch, and I.-O. Stamatescu, *Decoherence and the appearance of a classical world in quantum theory* (Springer Science & Business Media, 2013).
- [12] A. J. Leggett and A. Garg, Quantum mechanics versus macroscopic realism: Is the flux there when nobody looks?, *Phys. Rev. Lett.* **54**, 857 (1985).
- [13] A. J. Leggett, Realism and the physical world, *Reports on Progress in Physics* **71**, 022001 (2008).
- [14] A. J. Leggett, Realism and the physical world, in *Quantum Theory: A Two-Time Success Story*, edited by D. C. Struppa and J. M. Tollaksen (Springer Milan, Milano, 2014) pp. 9–20.
- [15] A. Palacios-Laloy, F. Mallet, F. Nguyen, P. Bertet, D. Vion, D. Esteve, and A. N. Korotkov, Experimental violation of a bell's inequality in time with weak measurement, *Nature Physics* **6**, 442 (2010).
- [16] V. Athalye, S. S. Roy, and T. S. Mahesh, Investigation of the leggett-garg inequality for precessing nuclear spins, *Phys. Rev. Lett.* **107**, 130402 (2011).
- [17] H. Katiyar, A. Shukla, K. R. K. Rao, and T. S. Mahesh, Violation of entropic leggett-garg inequality in nuclear spins, *Phys. Rev. A* **87**, 052102 (2013).
- [18] G. Waldherr, P. Neumann, S. F. Huelga, F. Jelezko, and J. Wrachtrup, Violation of a temporal bell inequality for single spins in a diamond defect center, *Phys. Rev. Lett.* **107**, 090401 (2011).
- [19] C. Budroni, T. Moroder, M. Kleinmann, and O. Gühne, Bounding temporal quantum correlations, *Phys. Rev. Lett.* **111**, 020403 (2013).
- [20] T. Fritz, Quantum correlations in the temporal clausen–horne–shimony–holt (chsh) scenario, *New Journal of Physics* **12**, 083055 (2010).
- [21] C. Budroni and C. Emary, Temporal quantum correlations and leggett-garg inequalities in multilevel systems, *Phys. Rev. Lett.* **113**, 050401 (2014).
- [22] K. Wang, C. Emary, X. Zhan, Z. Bian, J. Li, and P. Xue, Enhanced violations of leggett-garg inequalities in an experimental three-level system, *Optics express* **25**, 31462 (2017).
- [23] H. Katiyar, A. Brodutch, D. Lu, and R. Laflamme, Experimental violation of the leggett–garg inequality in a three-level system, *New Journal of Physics* **19**, 023033 (2017).
- [24] H. S. Karthik, H. Akshata Shenoy, and A. R. U. Devi, Leggett-garg inequalities and temporal correlations for a qubit under pt-symmetric dynamics, *Phys. Rev. A* **103**, 032420 (2021).
- [25] A. V. Varma, J. E. Muldoon, S. Paul, Y. N. Joglekar, and S. Das, Extreme violation of the leggett-garg inequality in nonunitary dynamics with complex energies, *Phys. Rev. A* **108**, 032202 (2023).
- [26] P. Lu, X. Rao, T. Liu, Y. Liu, J. Bian, F. Zhu, and L. Luo, Experimental demonstration of enhanced violations of leggett-garg inequalities in a pt-symmetric trapped-ion qubit, *Phys. Rev. A* **109**, 042205 (2024).
- [27] C.-W. Wu, M.-C. Zhang, Y.-L. Zhou, T. Chen, R. Huang, Y. Xie, B.-Q. Ou, W. Wu, A. Miranowicz, J. Zhang, *et al.*, Maximizing temporal quantum correlation by approaching an exceptional point, *arXiv preprint arXiv:2304.06590* (2023).
- [28] O. Moussa, C. A. Ryan, D. G. Cory, and R. Laflamme, Testing contextuality on quantum ensembles with one clean qubit, *Phys. Rev. Lett.* **104**, 160501 (2010).
- [29] J. Cavanagh, *Protein NMR spectroscopy: principles and practice* (Academic press, 1996).
- [30] M. H. Levitt, *Spin dynamics: basics of nuclear magnetic resonance* (John Wiley & Sons, 2008).
- [31] D. G. Cory, A. F. Fahmy, and T. F. Havel, Ensemble quantum computing by nmr spectroscopy, *Proceedings of the National Academy of Sciences* **94**, 1634 (1997).
- [32] N. A. Gershenfeld and I. L. Chuang, Bulk spin-resonance quantum computation, *science* **275**, 350 (1997).
- [33] D. G. Cory, M. D. Price, and T. F. Havel, Nuclear magnetic resonance spectroscopy: An experimentally accessible paradigm for quantum computing, *Physica D: Non-linear Phenomena* **120**, 82 (1998).
- [34] J. D. Roberts, The bloch equations. how to have fun calculating what happens in nmr experiments with a personal computer, *Concepts in Magnetic Resonance* **3**, 27 (1991).
- [35] D. A. Lidar, Lecture notes on the theory of open quantum systems, *arXiv preprint arXiv:1902.00967* [10.48550/arXiv.1902.00967](https://arxiv.org/abs/1902.00967) (2019).
- [36] H.-P. Breuer and F. Petruccione, *The theory of open quantum systems* (Oxford University Press, USA, 2002).